Finite Size Effects in Submonolayer Catalysts Investigated by CO Electrosorption on Pt$_{sML}$/Pd(100)

Qiuyi Yuan,[‡] Hieu A. Doan,[†] Lars C. Grabow,*[,†] and Stanko R. Brankovic*[,†,‡]

[†]Department of Chemical and Biomolecular Engineering and [‡]Department of Electrical and Computer Engineering, University of Houston, Houston, Texas 77204, United States of America

S *Supporting Information*

ABSTRACT: A combination of scanning tunneling microscopy, subtractively normalized interfacial Fourier transform infrared spectroscopy (SNIFTIRS), and density functional theory (DFT) is used to quantify the local strain in 2D Pt clusters on the 100 facet of Pd and its effect on CO chemisorption. Good agreement between SNIFTIRS experiments and DFT simulations provide strong evidence that, in the absence of coherent strain between Pt and Pd, finite size effects introduce local compressive strain, which alters the chemisorption properties of the surface. Though this effect has been widely neglected in prior studies, our results suggest that accurate control over cluster sizes in submonolayer catalyst systems can be an effective approach to fine-tune their catalytic properties.

The ultimate configuration of ultrathin catalyst overlayers in terms of catalyst utilization and specific activity is the 2D monolayer (ML). Catalyst MLs on different substrates have been extensively studied and their catalytic properties depend on the interplay between the host metal and the overlayer.[1−8] Their overall behavior is well described by the position of the energy level of *d*-band center (e_d) with respect to the Fermi level.[9] In the case of a substrate with weak electronic effect (weak ligand), e_d is mainly affected by the coherent strain (ε_{coh}) caused by the lattice constant mismatch between the overlayer and the substrate.[10] For substrates that are stronger ligands, the electronic and strain effects are coupled and e_d is a function of both.[9,11]

Ideal ML catalysts are difficult to synthesize and often exhibit defect structures that may contribute to their catalytic activity.[12] The most common catalyst is Pt, and at room temperature, Pt is very difficult to deposit in a true continuous ML configuration.[13] Hence, the submonolayer (sML) configuration is dominant. Functional Pt sML catalysts have a morphology consisting of compact 2D nanoclusters with certain size distribution and coverage of the substrate.[14−17] Because of finite size effects,[18,19] each 2D Pt nanocluster experiences a size-dependent compressive stress.[20] Thus, the local strain in Pt nanoclusters (ε_l) is a combination of the coherent strain and the strain caused by the finite size effects. Recent studies show that finite size effects enhance the bifunctional activity of RuPt core-edge clusters for CO electro-oxidation[21] and can significantly influence the activity of Pt sML (Pt$_{sML}$/Au-(111)).[22]

For substrates with a stronger electronic effect, the importance of finite size effects on the Pt sML activity has not been evaluated yet. A system that falls into this category is Pt sML on Pd substrate (Pt$_{sML}$/Pd(hkl)),[9,11] which has been identified as one of the best oxygen reduction catalysts[23] with significant practical application in fuel cell technology.[24] An added peculiarity of this system is the good lattice match, and hence, the absence of significant epitaxial strain. Therefore, it is of fundamental and practical significance to better understand the relative contribution of finite size effects on the catalytic behavior of Pt$_{sML}$/Pd(hkl). We address this challenge by studying carbon monoxide (CO) adsorption on well-characterized Pt$_{sML}$/Pd(100) electrode morphology using subtractively normalized interfacial Fourier transform infrared spectroscopy (SNIFTIRS) and density functional theory (DFT) calculations.

All solutions were made from ultrahigh purity chemicals and 18.2 MΩ ultrapure water. Potentials are quoted with respect to a saturated calomel electrode (SCE). The Pd and Pt single crystal electrodes were 2 mm thick disks with 10 mm in diameter supplied by Monocrystals Company. Preparation of the Pt(100) and Pd(100) surfaces followed a standard procedure for Pt-like metals described in the literature.[25] The Pt sML is deposited on Pd(100) using surface limited redox replacement (SLRR) of an underpotentially deposited (UPD) Cu ML.[15,26] After Pt sML deposition, up to 20 STM images are recorded at different terrace sites and analyzed using a customized digital image processing algorithm.[27,28] This provided information about the average and mean size of Pt nanoclusters, their height and coverage as descriptors of the Pt$_{sML}$/Pd(100) morphology. The details of the cell for in situ IR spectro-electrochemical measurements are described elsewhere.[29] The 128 scans with 4 cm^{-1} resolution are added in a single step. Spectra are given as $-\Delta R/R$ using the spectrum at the highest potential as the reference one. Prior to our experiments, the CO ML is adsorbed at the electrode surface from CO-saturated 0.1 M HClO$_4$. The solution in the attenuated total reflection cell is then purged by ultrapure Ar for 2 h to remove the remaining CO from the bulk solution. The analysis of the representative STM image of Pt$_{sML}$/Pd(100) obtained by SLRR of a Cu UPD ML in Figure 1A indicates that >94 ± 2% of the Pd(100) surface terrace sites are covered with Pt nanoclusters. Almost all of them are 2D (>98%) and have a compact shape. The corresponding
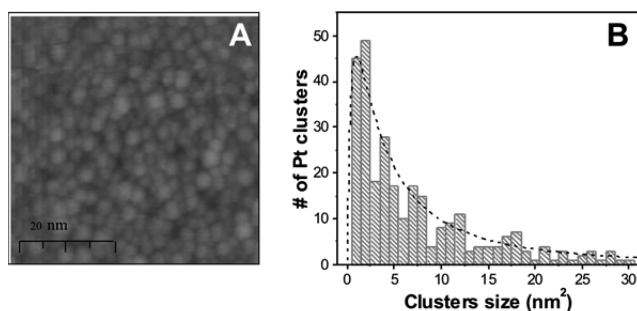
Figure 1. (A) Representative STM image of $Pt_{sML}/Pd(100)$. (B) Histogram of Pt nanoclusters' size distribution. The dashed line represents the fit of the log-normal distribution curve.

Figure 2. (A) SNIFTIRS data obtained at 0.1 V. The CO admission potential is −0.1 V and the reference spectra are taken at 0.6 V. (B) Shift of the CO adsorption peak position as a function of electrode potential.

histogram of the size distribution of 2D Pt nanoclusters is shown in Figure 1B.

The mean cluster size is found to be ≈4 nm², or ca. 50 Pt atoms in the nanocluster. This nanocluster size is assumed to be representative of the $Pt_{sML}/Pd(100)$ morphology and is used for further analyses of our SNIFTIRS and DFT results. Periodic DFT calculations were performed using the Vienna ab initio simulation package (VASP)[30−33] with the GGA-RPBE exchange correlation functional.[34] To estimate local strain we used a $Pt_{sML}/Pd(100)$ model consisting of a 52-atom 2D Pt-nanocluster supported on a four-layer (10 × 10) unit cell of Pd(100), of which the bottom two layers were fixed.

An adsorbed CO molecule forms σ and π bonds with a Pt surface. The latter one represents predominant contribution to the adsorption process.[11,35] The π bond is formed through back-donation of d-electrons from Pt into the π^*-antibonding molecular orbital of CO. Changes in e_d of Pt influence the strength of Pt—CO and C=O bonds simultaneously,[11] and can be measured indirectly through changes in the stretching frequency of the C=O bond of an adsorbed CO molecule. Shifts in the stretching band of CO for a particular bonding configuration on Pt toward higher wave numbers can be interpreted as decreased strength of the Pt—CO bond.[11] Along this concept, we consider the SNIFTIRS data for CO adsorption on Pt(100), Pd(100), and $Pt_{sML}/Pd(100)$ shown in Figure 2. The CO admission potential was −0.1 V, at which surface saturation is expected.[36,37] The reference spectra are taken at 0.6 V where no CO is present on the Pt surface.[38] For comparative analyses we used SNIFTIR spectra recorded at E = 0.1 V for these three surfaces shown in Figure 2A. At this potential, the effect of surface water in the double layer on the strength of the Pt—CO bond is expected to be minimal.[37,39] The spectra recorded at higher and lower potentials are presented as Figure S3. The positive stretching bands centered at ν = 2081 and ν = 2064 cm⁻¹ are associated with the on-top, linear bonding configuration of CO molecules to $Pt_{sML}/Pd(100)$ and Pt(100) surfaces, $\nu(CO_L)$, Figure 2A. Spectra recorded at the same potential for Pd(100) indicate a stretching band centered at 1962 cm⁻¹ corresponding to bridge bonded CO, $\nu(CO_B)$. The SNIFTIRS data for Pt(100) and Pd(100) are in agreement with previous studies for these surfaces.[37,40] The ≈20 cm⁻¹ shift of $\nu(CO_L)$ to higher wave numbers for $Pt_{sML}/Pd(100)$ as compared to Pt(100) indicates a significantly stronger C=O bond and weaker Pt—CO bond for CO molecules adsorbed on $Pt_{sML}/Pd(100)$. This trend is preserved over a wide range of potentials, from −0.1 V up to 0.4 V. At E = 0.5 V, the adsorption band for CO on the $Pt_{sML}/Pd(100)$ surface is no longer detected, suggesting that CO has desorbed
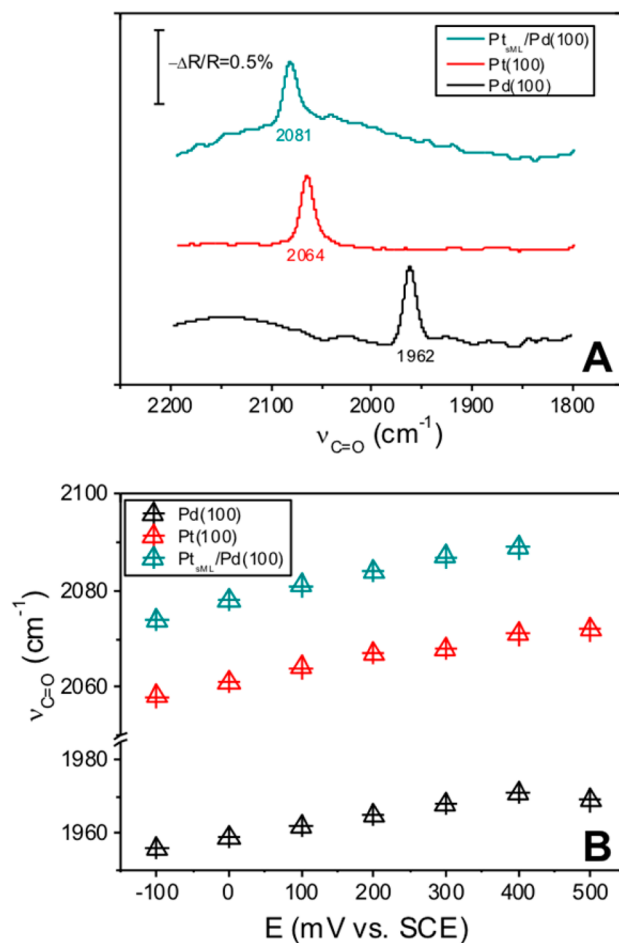
from the surface. However, at the same potential, CO is detected on both Pt(100) and Pd(100), Figure 2B. The observed difference in $\nu(CO_L)$ for $Pt_{sML}/Pd(100)$ and Pt(100) could be explained by repulsive lateral interactions in the adsorbed CO layer if its coverage varies between these two surfaces.[35,37,41] A recent STM study of CO adsorption on Pt(100) shows that in the vicinity of surface defects such as steps a lower CO coverage is observed ($c(2 \times 2)$−2CO, θ_{CO} = 0.5 ML) than on terraces ($c(2 \times 6)$−10CO, θ_{CO} = 0.83 ML).[36] Considering that $Pt_{sML}/Pd(100)$ consists of 2D nanoclusters with a considerably high density of Pt cluster edges, a lower CO coverage can be anticipated on $Pt_{sML}/Pd(100)$ compared to Pt(100) at the same potential. In contrast to our experimental data, the coverage effect alone should yield stronger binding and $\nu(CO_L)$ with lower wavenumber for $Pt_{ML}/Pd(100)$ than on Pt(100).[11] Furthermore, the same tuning rate (Stark shift) measured for both surfaces in the potential range between −0.1 and +0.2 V (30 ± 3 cm⁻¹ V⁻¹) suggests that the CO coverage on both surfaces is approximately equal,[37] Figure 2B. The same conclusion can be derived by comparing the area under the stretching bands of CO for Pt(100) and $Pt_{sML}/Pt(100)$ surfaces. Therefore, the observed difference in $\nu(CO_L)$ and narrower potential range of CO stability on $Pt_{sML}/Pd(100)$ are interpreted as evidence for a weaker Pt—CO bond on $Pt_{sML}/Pd(100)$ than on Pt(100). The extended conclusion from our

SNIFTIRS data is that e_d for $Pt_{sML}/Pd(100)$ is shifted away from the Fermi level.

The above statement and experimental results are in partial disagreement with earlier DFT studies of the $Pt_{ML}/Pd(hkl)$ system.[9,11] Those studies predict only a mild shift of e_d, which suggests no significant difference in Pt—CO bond strength between the $Pt_{ML}/Pd(100)$ and $Pt(100)$ surface.[11] However, the previous theoretical work considered a continuous Pt ML over Pd where ε_{coh} is determined by the epitaxial lattice mismatch between Pt and Pd ($\varepsilon_{coh} = -0.85\%$),[42] whereas for 2D Pt nanoclusters the average amount of strain $<\varepsilon>$ is expected to be quite different from ε_{coh} due to the finite size effect.

Figure 3A shows a calculated strain map for a 52-atom Pt nanocluster on Pd(100) with a realistic diameter of ca. 2 nm.
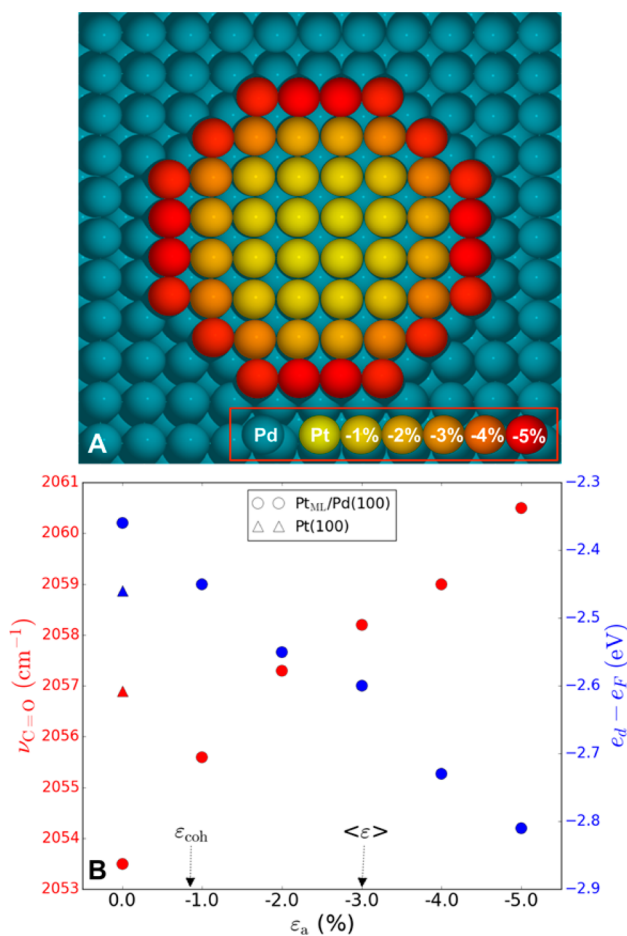
Figure 3. (A) Strain map of the 52-atom Pt nanocluster on Pd(100). (B) Calculated values of the C=O stretching frequency (red) for linearly adsorbed CO molecules (θ_{CO} = 0.5 ML) and d-band centers (blue) of Pt atoms on the $Pt_{ML}/Pd(100)$ and $Pt(100)$ surfaces as a function of applied lateral strain ε_a.

The local strain, ε_l, exhibits a strong radial dependence[20] and ranges between −5.0% at the periphery to ~0% in the center of the nanocluster. As described in the SI we extracted the average strain in the Pt nanocluster, $<\varepsilon>$, which we use to quantify the overall strain state in the $Pt_{sML}/Pd(100)$ system. We note that the obtained value for $<\varepsilon> = -3.0\%$ is about 4 times larger as compared to the coherent strain ε_{coh}. We then used smaller commensurate (2 × 2) unit cells to compare the C=O stretching frequency on Pt(100), Pd(100), and Pt/Pd(100)

surfaces. The resulting C=O stretching frequency at θ_{CO} = 0.5 ML and the corresponding d-band centers of Pt atoms on $Pt_{ML}/Pd(100)$ surface as a function of applied lateral strain ε_a are shown in Figure 3B. The corresponding CO binding energies are provided in Figure S3, and we also verified that the coverage dependent frequencies obtained for the continuous Pt ML models converge to the result obtained for the 52-atom $Pt_{sML}/Pd(100)$ model in the absence of induced strain (Table S1, Figure S4).

In the absence of strain, the calculated value of $\nu(CO_L)$ for $Pt_{ML}/Pd(100)$ is 2053.5 cm^{-1}, and lower than for Pt(100) (2057 cm^{-1}). The lower wavenumber represents the shift in the direction toward the value of $\nu(CO_L)$ of Pd(100) (1900 cm^{-1}), Figure 3B, and is consistent with the ligand effect discussed in previous DFT studies.[11] The introduction of compressive lateral strain leads to a weakening of the Pt—CO bond and an increase of $\nu(CO_L)$, which counteracts the ligand effect. At an average compressive strain of ca. −2% $\nu(CO_L)$ for $Pt_{ML}/Pd(100)$ and Pt(100) are essentially equal. Further increase of the compressive strain leads to an approximately linear increase of $\nu(CO_L)$, Figure 3B, ultimately predicting a higher $\nu(CO_L)$ for $Pt_{ML}/Pd(100)$ than for Pt(100). Notably, for strain levels equal or higher than the value of $<\varepsilon>$, we calculated $\nu(CO_L) \geq$ 2058 cm^{-1}, which is in good qualitative agreement with the experimental observations in Figure 2. Moreover, the calculated Stark shift for $Pt_{ML}/Pd(100)$ with $\varepsilon_a = -3\%$ extracted from data in Figure S5 is 28.4 ± 1.3 cm^{-1} V^{-1} Å. Similarly, the tuning rates for Pt(100) and Pd(100) in Figure 2B are 31.0 ± 0.3 cm^{-1} V^{-1} Å and 34.0 ± 0.6 cm^{-1} V^{-1} Å, respectively. Indeed, the good agreement of the simulated and measured Stark shift instills confidence in the computational model, and particularly, the surface coverage. Hence, we conclude that the experimentally observed trend in Figure 2 is recovered when the applied strain used in DFT calculations approaches the value of $<\varepsilon>$, rather than the coherent strain ε_{coh}. This analysis indicates that finite size effects play a dominant role in explaining the energetics of the CO adsorption process on $Pt_{sML}/Pd(100)$ surfaces.

The presented experimental and theoretical results provide clear evidence that the morphology of Pt_{sML} is important in determining their overall catalytic activity. This fact has not been considered in previous reports.[15,23,24] Here reported finite size effects represent a phenomenon that can be used as additional knob to fine-tune the d-band energy, which inherently controls overall catalytic activity. Turning this knob in the desired direction by varying nanocluster sizes requires a better understanding of the conditions during ML catalyst synthesis, which are responsible for nanocluster size control.[43,44] Future efforts in this direction are a promising route to provide a better correlation between ML catalyst synthesis procedures and their resulting catalytic behavior.

■ ASSOCIATED CONTENT

ⓢ Supporting Information

The Supporting Information is available free of charge on the ACS Publications website at DOI: 10.1021/jacs.7b08740.

Full spectra corresponding to Figure 2b with detailed description of experimental procedures and calculation methods (PDF)

AUTHOR INFORMATION

Corresponding Authors

*SRBrankovic@uh.edu
*grabow@uh.edu

ORCID ⦿

Lars C. Grabow: 0000-0002-7766-8856

Notes

The authors declare no competing financial interest.

ACKNOWLEDGMENTS

REFERENCES

(1) Yu, W.; Porosoff, M. D.; Chen, J. G. *Chem. Rev.* **2012**, *112*, 5780.

(2) Greeley, J.; Mavrikakis, M. *Nat. Mater.* **2004**, *3*, 810.

(3) Alayoglu, S.; Nilekar, A. U.; Mavrikakis, M.; Eichhorn, B. *Nat. Mater.* **2008**, *7*, 333.

(4) Knudsen, J.; Nilekar, A. U.; Vang, R. T.; Schnadt, J.; Kunkes, E. L.; Dumesic, J. A.; Mavrikakis, M.; Besenbacher, F. *J. Am. Chem. Soc.* **2007**, *129*, 6485.

(5) Xu, Y.; Ruban, A. V.; Mavrikakis, M. *J. Am. Chem. Soc.* **2004**, *126*, 4717.

(6) Rossmeisl, J.; Ferrin, P.; Tritsaris, G. A.; Nilekar, A. U.; Koh, S.; Bae, S. E.; Brankovic, S. R.; Strasser, P.; Mavrikakis, M. *Energy Environ. Sci.* **2012**, *5*, 8335.

(7) Loukrakpam, R.; Yuan, Q.; Petkov, V.; Gan, L.; Rudi, S.; Yang, R.; Huang, Y.; Brankovic, S. R.; Strasser, P. *Phys. Chem. Chem. Phys.* **2014**, *16*, 18866.

(8) Erini, N.; Loukrakpam, R.; Petkov, V.; Baranova, E. A.; Yang, R.; Teschner, D.; Huang, Y.; Brankovic, S. R.; Strasser, P. *ACS Catal.* **2014**, *4*, 1859.

(9) Ruban, A.; Hammer, B.; Stoltze, P.; Skriver, H. L.; Nørskov, J. K. *J. Mol. Catal. A: Chem.* **1997**, *115*, 421.

(10) Mavrikakis, M.; Hammer, B.; Nørskov, J. K. *Phys. Rev. Lett.* **1998**, *81*, 2819.

(11) Bligaard, T.; Nørskov, J. K. *Electrochim. Acta* **2007**, *52*, 5512.

(12) Greeley, J.; Mavrikakis, M. *Catal. Today* **2006**, *111*, 52.

(13) Waibel, H. F.; Kleinert, M.; Kibler, L. A.; Kolb, D. M. *Electrochim. Acta* **2002**, *47*, 1461.

(14) Brankovic, S. R.; Wang, J. X.; Adžić, R. R. *Electrochem. Solid-State Lett.* **2001**, *4*, A217.

(15) Brankovic, S.; Wang, J.; Adžić, R. *Surf. Sci.* **2001**, *474*, L173.

(16) Park, S.; Yang, P.; Corredor, P.; Weaver, M. J. *J. Am. Chem. Soc.* **2002**, *124*, 2428.

(17) Liu, Y.; Gokcen, D.; Bertocci, U.; Moffat, T. P. *Science* **2012**, *338*, 1327.

(18) Li, L.; Larsen, A. H.; Romero, N. A.; Morozov, V. A.; Glinsvad, C.; Abild-Pedersen, F.; Greeley, J.; Jacobsen, K. W.; Nørskov, J. K. *J. Phys. Chem. Lett.* **2013**, *4*, 222.

(19) *Quantum Phenomena in Clusters and Nanostructures*; Khana, S. N., Castleman, A. W., Eds.; Springer: New York, 2003.

(20) Kern, R.; Müller, P. *Surf. Sci.* **1997**, *392*, 103.

(21) Grabow, L. C.; Yuan, Q.; Doan, H. A.; Brankovic, S. R. *Surf. Sci.* **2015**, *640*, 50.

(22) Bae, S.-E.; Gokcen, D.; Liu, P.; Mohammadi, P.; Brankovic, S. R. *Electrocatalysis* **2012**, *3*, 203.

(23) Zhang, J. L.; Vukmirovic, M. B.; Xu, Y.; Mavrikakis, M.; Adžić, R. R. *Angew. Chem., Int. Ed.* **2005**, *44*, 2132.

(24) Adžić, R.; Zhang, J.; Sasaki, K.; Vukmirovic, M.; Shao, M.; Wang, J.; Nilekar, A.; Mavrikakis, M.; Valerio, J.; Uribe, F. *Top. Catal.* **2007**, *46*, 249.

(25) Clavilier, J.; Faure, R.; Guinet, G.; Durand, R. *J. Electroanal. Chem. Interfacial Electrochem.* **1980**, *107*, 205.

(26) Zhang, J.; Mo, Y.; Vukmirovic, M. B.; Klie, R.; Sasaki, K.; Adzic, R. R. *J. Phys. Chem. B* **2004**, *108*, 10955.

(27) Tripathi, A. The new image processing algorithm for qualitative and quantitative STM image data analysis. Master's Thesis, University of Houston, Houston, TX, 2012.

(28) Otsu, N. *IEEE Trans. Syst. Man. Cybern* **1979**, *9*, 62.

(29) Marinković, N. S.; Hecht, M.; Loring, J. S.; Fawcett, W. R. *Electrochim. Acta* **1996**, *41*, 641.

(30) Blöchl, P. E. *Phys. Rev. B: Condens. Matter Mater. Phys.* **1994**, *50*, 17953.

(31) Kresse, G.; Furthmüller, J. *Comput. Mater. Sci.* **1996**, *6*, 15.

(32) Kresse, G.; Furthmüller, J. *Phys. Rev. B: Condens. Matter Mater. Phys.* **1996**, *54*, 11169.

(33) Kresse, G.; Joubert, D. *Phys. Rev. B: Condens. Matter Mater. Phys.* **1999**, *59*, 1758.

(34) Hammer, B.; Hansen, L.; Nørskov, J. *Phys. Rev. B: Condens. Matter Mater. Phys.* **1999**, *59*, 7413.

(35) Wasileski, S. A.; Koper, M. T. M.; Weaver, M. J. *J. Phys. Chem. B* **2001**, *105*, 3518.

(36) Wakisaka, M.; Yoneyama, T.; Ashizawa, S.; Hyuga, Y.; Ohkanda, T.; Uchida, H.; Watanabe, M. *Phys. Chem. Chem. Phys.* **2013**, *15*, 11038.

(37) Chang, S.-C.; Weaver, M. J. *J. Phys. Chem.* **1990**, *94*, 5095.

(38) Markovic, N. M.; Lucas, C. A.; Grgur, B. N.; Ross, P. N. *J. Phys. Chem. B* **1999**, *103*, 9616.

(39) Iwasita, T.; Xia, X. *J. Electroanal. Chem.* **1996**, *411*, 95.

(40) Zou, S.; Gómez, R.; Weaver, M. *Langmuir* **1999**, *15*, 2931.

(41) Grabow, L. C.; Hvolbæk, B.; Nørskov, J. K. *Top. Catal.* **2010**, *53*, 298.

(42) Cullity, B. D.; Stock, S. R. *Elements of X-Ray Diffraction*; 3rd ed.; Prentice-Hall: New York, 2001.

(43) Gokcen, D.; Yuan, Q.; Brankovic, S. R. *J. Electrochem. Soc.* **2014**, *161*, D3051.

(44) Bulut, E.; Wu, D.; Dole, N.; Kilic, H.; Brankovic, S. R. *J. Electrochem. Soc.* **2017**, *164*, D159.